Manipulating chiral microswimmers in a channel

Yunyun Li,[1] Pulak K. Ghosh,[2] Fabio Marchesoni,[3] and Baowen Li[1,4]

[1]*Center for Phononics and Thermal Energy Science, School of Physics Science and Engineering, Tongji University, Shanghai 200092, People's Republic of China*

[2]*Department of Chemistry, Presidency University, Kolkata 700073, India*

[3]*Dipartimento di Fisica, Università di Camerino, I-62032 Camerino, Italy*

[4]*Department of Physics and Center for Computational Science and Engineering, National University of Singapore, Singapore 117456, Singapore*

(Received 10 August 2014; published 2 December 2014)

We numerically simulate the diffusion of overdampd pointlike Janus particles along narrow two-dimensional periodically corrugated channels with reflecting walls. The self-propulsion velocity of the particle is assumed to rotate subject to an intrinsic bias modeled by a torque. Breaking the mirror symmetry of the channel with respect to its axis suffices to generate a directed particle flow with orientation and magnitude which depend on the channel geometry and the particle swimming properties. This means that chiral microswimmers drift autonomously along a narrow channel under more general asymmetry conditions than previously reported, a property of potential impact on their fabrication and technological applications.

DOI: 10.1103/PhysRevE.90.062301 PACS number(s): 82.70.Dd, 36.40.Wa, 87.15.hj

I. INTRODUCTION

Active Brownian particles, also known as microswimmers, are self-propelled micro- and nanoobjects capable of directed random motion. Actually, self-propulsion [1] is the ability of most living organisms to move in the absence of external drives by means of an internal "engine" of their own. Recently, a new type of artificial microswimmer has been fabricated [2], where self-propulsion is powered by local gradients the particles themselves generate, when coupled to an external energy source (self-phoretic effects) [3]. Typically, such particles consist of two distinct "faces," only one of which is chemically or physically active and for this reason are dubbed Janus particles (JPs) [4]. Such swimmers thus harvest energy from their environment through an external "engine," which may involve concentration gradients (by catalyzing a chemical reaction on their active surface [5,6]) as well as thermal gradients (e.g., by inhomogeneous light absorption [7,8] or magnetic excitation [9]).

The self-propulsion mechanism acts on the microswimmer by means of an *effective* force and, possibly, a torque [10]. In the absence of a torque, the line of motion is directed parallel to the self-phoretic force and the JP propels itself along a straight line, until it changes direction, due to gradient fluctuations [3] or random collisions against other particles or geometric boundaries [11]. This is the highly stylized case mostly studied in the recent literature, where, for simplicity, the JPs are assumed to be rotationally symmetric around their line of motion (symmetric JPs). In the presence of an additional torque, the self-phoretic force and the line of motion are no longer aligned and the microswimmer tends to execute circular orbits [10,12] (chiral microswimmer). Active chiral motion has long been known in biology [10,13,14] and more recently observed in asymmetrically propelled artificial micro- and nanorods: A torque can be intrinsic to the propulsion mechanism, due to the presence of geometrical asymmetries in the particle fabrication, engineered or accidental (asymmetric JPs) [15–17], or externally applied, for instance, by laser irradiation [7] or hydrodynamic fields [18]. In the finite damping regime, the Lorentz force exerted by a magnetic field on a charged active Brownian particle also amounts to an external torque [19,20].

Controlling transport of *artificial* microswimmers and JPs, in particular, through confined geometries is of utmost importance for the application of microswimmer technology to science and engineering [21,22]. The rectification of *nonchiral* JPs through periodic arrays [8] and channels [23] surely is a suggestive option. Such devices do operate autonomously, that is, in the absence of external drives or gradients, but at the price of a strict fabrication requirement: Their geometry must be asymmetric under mirror reflection in the direction of the output current [22].

In this paper we show by a combination of numerical simulations and analytical arguments, that *chiral* JPs are susceptible to being autonomously rectified in narrow corrugated channels under more general symmetry breaking conditions than suggested by the one-dimensional reduction formalisms [22,24]. As shown in Sec. III a sufficient condition is that the cylindrical (in three dimensions, 3D) or mirror symmetry of the channel with respect to its axis (in two dimensions, 2D) be broken. This is the net effect of opposed boundary flows, which set on as the particle orients its self-propulsion velocity tangentially to the channel walls. This phenomenon allows one, in principle, to design a distinct class of active particle rectifiers, where, in contrast with the better known ratchet technology [22], spatial asymmetry in the direction of propagation would be unnecessary. The mechanism investigated here not only enhances transport of JPs in general, but also allows an accurate control of their flows; how the JP rectification power depends on the self-propulsion parameters and channel geometry is discussed in Sec. IV. In Sec. V we briefly discuss similarities and differences with the transport properties of a nonchiral JP of unit charge moving along a 2D channel, subject to the external torque exerted by a constant orthogonal magnetic field. In the concluding Sec. VI we suggest simple sorting techniques for chiral JPs based on their swimming

properties, a key property for the fabrication and application of chiral artificial microswimmers at large.

II. MODEL

In order to avoid unessential complications, we restrict this paper to the case of 2D channels and pointlike artificial microswimmers. The extension of our key conclusions to 3D channels and finite-size particles is also possible [14]. A chiral JP gets a continuous push from the suspension fluid, which in the overdamped regime (for pointlike swimmers hydrodynamic effects [25,26] and particle-particle collisions are negligible [27]) amounts to a rotating self-propulsion velocity $\mathbf{v}_0$ with constant modulus v_0 and angular velocity Ω. Additionally, the self-propulsion direction varies randomly with time constant τ_θ, under the combined action of thermal noise and fluctuations intrinsic to the self-propulsion mechanism. Accordingly, the microswimmer mean free self-propulsion path approximates a circular arc of radius $R_\Omega = v_0/|\Omega|$ and length $l_\theta = v_0\tau_\theta$ [12].

The bulk dynamics of such a chiral JP obeys the Langevin equations [12]

$$\begin{aligned} \dot{x} &= v_0 \cos\theta + \xi_x(t), \\ \dot{y} &= v_0 \sin\theta + \xi_y(t), \\ \dot{\theta} &= \Omega + \xi_\theta(t), \end{aligned} \tag{1}$$

where the particle center of mass is confined into the plane (x,y), subject to equilibrium thermal fluctuations modeled by the Gaussian noises $\xi_i(t)$ with $\langle \xi_i(t)\rangle = 0$ and $\langle \xi_i(t)\xi_j(0)\rangle = 2D_0\delta_{ij}\delta(t)$ for $i = x,y$. The channel is directed along the x axis, the self-propulsion velocity is oriented at an angle θ with respect to it, and the sign of Ω coincides with the positive (levogyre) and negative (dextrogyre) chirality of the swimmer. As explained in Sec. I, we refer to Ω as a torque. The fluctuations of the propulsion direction are modeled by the Gaussian noise $\xi_\theta(t)$ with $\langle \xi_\theta(t)\rangle = 0$ and $\langle \xi_\theta(t)\xi_\theta(0)\rangle = 2D_\theta\delta(t)$, where $D_\theta = 2/\tau_\theta$. In the bulk, self-propulsion contributes an additional amount $D_s = v_0^2\tau_\theta/4$ to the thermal diffusivity, D_0 [23,28]. The self-propulsion parameters, v_0 and Ω, model some self-phoretic mechanism acting on the particle, and not an external field of force; for this reason v_0 and Ω were taken as independently tunable. Analogously, we treated all noise sources in Eq. (1) also as independent, although thermal and orientational fluctuations may be, to some degree, statistically correlated (see, e.g., [14]). More importantly, the parameters used in our simulations are experimentally accessible, as apparent on expressing times in seconds and lengths in microns (see Refs. [8,14] for a comparison).

We numerically simulated the set of Langevin equations (1) for a levogyre microswimmer, $\Omega > 0$, confined to a periodic 2D channel,

$$\begin{aligned} w_+(x) &= \frac{1}{2}\left[\Delta + \epsilon(y_L - \Delta)\sin^2\left(\frac{\pi}{x_L}(x + x_0)\right)\right], \\ w_-(x) &= -\frac{1}{2}\left[\Delta + (y_L - \Delta)\sin^2\left(\frac{\pi}{x_L}x\right)\right], \end{aligned} \tag{2}$$

where x_L is the compartment length, Δ the pore size, and y_L the channel width. Two additional tunable geometrical parameters have been introduced in $w_+(x)$, namely, x_0 and ϵ with $\epsilon \geqslant 0$, respectively, to shift the position and tune the amplitude of the upper wall with respect to the lower one (Fig. 1). Simulating a constrained JP requires defining its collisional dynamics at the boundaries. For the translational velocity $\dot{\mathbf{r}}$ we assumed elastic reflection [24]. Regarding the coordinate θ, we assumed that it does not change upon collision (sliding boundary conditions (b.c.) [23]). As a consequence the active particle slides along the walls until either the orientational fluctuations, $\xi_\theta(t)$, or the torque, Ω, redirect it toward the interior of the compartment.

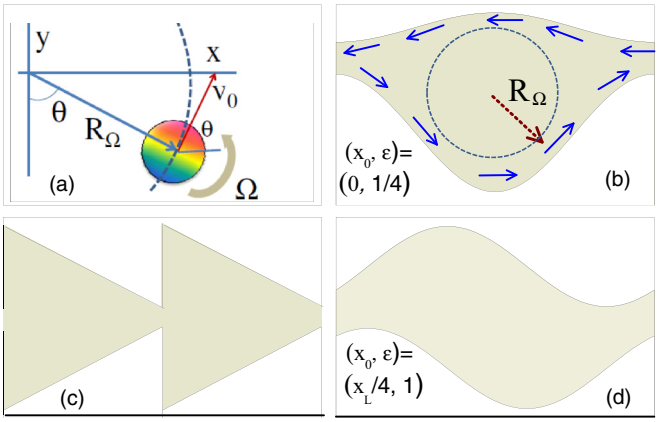

FIG. 1. (Color online) Chiral Janus particle in a narrow channel: (a) particle with velocity $\mathbf{v}_0$ and torque Ω, Eq. (1), and examples of periodically corrugated channels with different symmetry properties: (b) upside-down asymmetric and right-left symmetric; (c) right-left asymmetric and upside-down symmetric, and (d) centrosymmetric. Channel walls: (b) and (d) as in Eqs. (2) with ϵ and x_0 given in the legends; (c) the triangular wall profile of Ref. [23]. In (b) the open boundary trajectories and a closed circular trajectory of radius R_Ω are drawn for explanatory purposes (see Fig. 2 for actual simulation data).

In Figs. 3–5 we computed the directed flow, $\bar{v} = \lim_{t\to\infty}\langle x(t) - x(0)\rangle/t$, for different particle swimming properties and channel geometries. Equations (1) have been numerically integrated by using a standard Milstein algorithm [23] with short time step, 10^{-5}–10^{-7}, to ensure numerical stability. At start, $t = 0$, the particle was assumed to be uniformly distributed with random orientation in a channel compartment located between $x = 0$ and $x = x_L$. The running time was set to $10^4 \times \tau_\theta$, or $10^4 \times \Omega^{-1}$, or 10^4, whichever is greater, so as to neglect transient effects due to transients. The data points reported in the figures shown here have been obtained by ensemble averaging over a minimum of 10^4 trajectories.

III. CHIRAL RECTIFICATION

When confined to a channel compartment of size smaller than its self-propulsion length, l_θ, a chiral microswimmer tends to align its velocity parallel to the walls [8,15], thus generating two boundary flows oriented to opposite directions. This situation occurs at low noise (both thermal and orientational) when, upon increasing the torque, the particle tends to accumulate against the walls [23,29–31] with tangential velocities approaching $\pm v_0$. Optimal anomalous rectification [30] is thus established under the regime of strong chirality,

$|\Omega|\tau_\theta \gg 1$ or $l_\theta \gg R_\Omega$, and high Péclet numbers, $\mathrm{Pe} \gg 1$, with $\mathrm{Pe} \equiv v_0^2|\Omega|/D_0$. Releasing either of these conditions suppresses the channel rectification power. For instance, on lowering the torque, the chiral radius R_Ω eventually grows much larger than the compartment dimensions, $R_\Omega \gg x_L, y_L$; as a consequence, for $l_\theta \gg R_\Omega$, the swimmer spends more time drifting between the upper and lower walls than sliding along them, thus weakening the boundary flows. Vice versa, when either the self-propulsion length or the chiral radius are smaller than the compartment dimension, $l_\theta \ll x_L, y_L$ or $R_\Omega \ll x_L, y_L$, particle diffusion occurs mostly away from the boundaries. This implies that for high noise levels or exceedingly large torques the boundary rectification effects grow negligible.

These different chiral regimes are well illustrated in Fig. 2, where we plotted the stationary probability density, $P(x,y)$, of a JP diffusing in the sinusoidal channel of Fig. 1(b), namely, within the boundaries of Eq. (2) with $\epsilon = 0.25$ and $\Delta = 0.12$. For $\Omega = 10$, top panel, the particle tends to sojourn at the center of the compartment, where it gets trapped. Accordingly, the boundary flows through the pores are broken. Vice versa, for $\Omega = 0.1$, bottom panel, the particle trajectory tends to bounce between the upper and lower boundaries, so that the particle density piles up against the midsections of the compartment walls, mostly away from the pores. Both regimes of high and low chiral frequency in Fig. 2 clearly hint at a suppression of autonomous rectification, as explicitly demonstrated by the simulation data of Fig. 4. Finally, for $\Omega = 2$, the boundary flows are the strongest along both walls and, most importantly, across the pores. By the same token, the probability density at the center of the compartment gets uniformly depleted, which corresponds to the situation sketched in Fig. 1(b), where the chiral radius R_Ω is of the order of half the compartment length and the particle can thus trace a closed orbit inside the compartment.

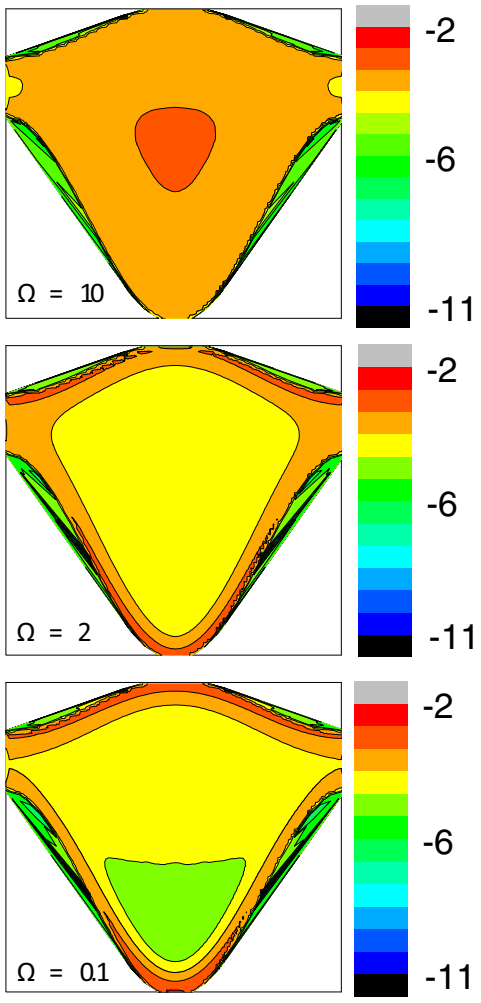

FIG. 2. (Color online) Logarithmic contour plots of the stationary particle density, $P(x,y)$, in a compartment of Eq. (2) with $x_L = y_L = 1$, $x_0 = 0$, $\Delta = 0.12$, and $\epsilon = 0.25$, for different values of Ω. Other simulation parameters are $\tau_\theta = 10$, $v_0 = 1$, and $D_0 = 0.01$. For $\Omega = 2$, central panel, the boundary flows are the strongest, as $P(x,y)$ gets uniformly depleted at the center of the compartment. This condition corresponds to a maximum in the rectification power of Fig. 4.

For $\Omega > 0$ the JP is levogyre, which means that the upper and lower boundary flows are oriented, respectively, to the left and right. It then becomes apparent that the net flow along the channel axis, $\bar{v}$, takes the sign of the flow along the less corrugated boundary, that is, $w_+(x)$ for $\epsilon < 1$ and $w_-(x)$ for $\epsilon > 1$ [see compartments of Figs. 1(b) and 1(d) and data of Fig. 3], and vanishes for $\epsilon = 1$. As long as rectification occurs at the boundary layers (with the channel compartments only

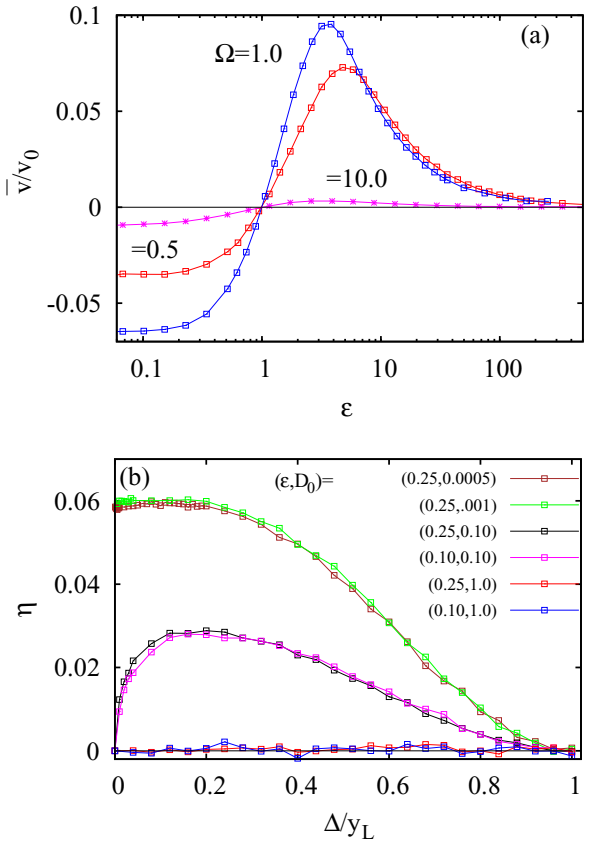

FIG. 3. (Color online) Rectification of a levogyre JP in the channel of Eq. (2): (a) $\bar{v}/v_0$ vs ϵ for $\Delta = 0.12$, $D_0 = 0.01$, and different Ω; (b) $\eta = |\bar{v}|/v_0$ vs Δ for $\Omega = 1$ and different ϵ, with $\epsilon < 1$, and D_0 (see legends). Note that here $\bar{v} = -|\bar{v}|$ and for a right-left symmetric channel, $\bar{v}(-\Omega) = -\bar{v}(\Omega)$. Other simulation parameters are $D_\theta = 0.3$, $v_0 = 1$, $x_0 = 0$, and $x_L = y_L = 1$.

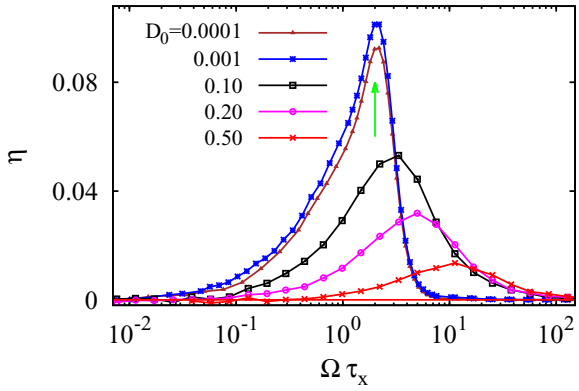

FIG. 4. (Color online) Optimization of the rectification of a levogyre JP with $v_0 = 1$ in the channel of Eq. (2) with $\epsilon = 0.25$, $x_0 = 0$, and $x_L = y_L = 1$: η vs $\Omega\tau_X$ for $\Delta = 0.12$, $\tau_\theta = 10$, and different D_0 (see legend). Here τ_X is the compartment crossing time, $\tau_X = x_L/v_0$, and the vertical arrow points to $\Omega_M\tau_X$.

sparsely traversed by the particle), the argument above sets a simple upper bound to the channel rectification power, $\eta = |\bar{v}|/v_0$, that is,

$$\eta \leqslant \frac{x_L}{2}\left|\frac{1}{s_+} - \frac{1}{s_-}\right|, \tag{3}$$

where $s_\pm$ are the lengths of the upper and lower compartment boundaries. This upper bound is actually approached under optimal rectification conditions, for instance, in Fig. 4, and modified to account for a different geometry, in Fig. 6 (see Sec. VI).

Symmetry requirements

In our interpretation the rectification process is governed by the boundary flows [20] and, therefore, by the spatial symmetry of the channel walls, rather than the pore geometry [14]. This picture is consistent with rigorous symmetry arguments. First of all we notice that the 2D channel compartments in Fig. 1 can be asymmetric under inversion of either the y axis ($y \to -y$, upside-down asymmetric), panel (b), of the x axis ($x \to -x$, right-left asymmetric), panel (c), or both, panel (d). The compartment (d), while both upside-down and right-left asymmetric, is invariant under any pair of x and y axis inversions, namely, it is centrosymmetric. With reference to the right-left symmetric compartment (b), we notice that Eqs. (1) are invariant under the transformations $x \to -x$ and $\theta \to \pi - \theta$ or, equivalently, $\Omega \to -\Omega$, which leaves the channel also invariant. As a consequence $\bar{v}(-\Omega) = -\bar{v}(\Omega)$. Similarly, in the case of the upside-down symmetric compartment (c), one concludes that $\bar{v}(\Omega) = \bar{v}(-\Omega)$. Moreover, for a centrosymmetric compartment both parity relations hold simultaneously; hence, $\bar{v}(\Omega) = 0$. This is the case of the channel of Eq. (2) for $\epsilon = 1$ and any x_0, for which we verified that $\bar{v}$ is identically zero. In view of the different chiral parity of $\bar{v}(\Omega)$ for compartments (b) and (c), it becomes apparent that a finite torque is a necessary condition for JP rectification in a right-left symmetric channel. Finally, by shifting the channel walls $w_\pm(x)$ in Eq. (2) by a length x_0, one can easily prove the additional symmetry relations $\bar{v}(x_0,\Omega) = -\bar{v}(-x_0, -\Omega)$ for right-left symmetric compartments, and $\bar{v}(x_0,\Omega) = \bar{v}(-x_0, -\Omega)$ for upside-down symmetric compartments. This symmetry relation is discussed in Sec. V for nonchiral JPs, $\Omega = 0$, diffusing in the channel of Eq. (2).

IV. RECTIFICATION POWER

The boundary flow mechanism explains well the dependence of $\bar{v}$ on the compartment parameters Δ and ϵ displayed in Fig. 3. In particular, we observe that (i) $\bar{v} \lessgtr 0$ for $\epsilon \lessgtr 1$ and any choice of Δ and Ω (with $\Omega > 0$) [Fig. 3(a)]; (ii) increasing the pore size, Δ, also enlarges the compartment volume, thus diminishing the statistical weight of the boundary layers; accordingly, $\bar{v}$ gets suppressed [Fig. 3(b)]; (iii) more remarkably, in the noiseless limit $\bar{v}$ is discontinuous at $\Delta = 0$, with $\bar{v} \neq 0$ for $\Delta \to 0$ and $\bar{v} = 0$ at $\Delta = 0$ [Fig. 3(b)]. This result stresses the prominent role of the boundary flows, whose width, for an overdamped pointlike JP, is vanishingly small; and (iv) for finite thermal noise levels η peaks at an optimal pore width [23].

Thermal noise affects the resonant behavior of $|\bar{v}|$ as a function of Ω reported in Fig. 4. The rectification power goes through a maximum for a certain value of the torque, without crossing the upper bound set in Eq. (3). On decreasing D_0, the peak shifts to the left until it settles around a limiting value, Ω_M, where it is the most pronounced. The peak frequency Ω_M can be estimated by noticing that on increasing Ω the chiral radius $R_\Omega = v_0/|\Omega|$ decreases until the microswimmer can perform a closed orbit (actually a logarithmic spiral with exponentially small steps [12]) inside the compartment, without being captured by the boundary layers [see Figs. 1(b) and 2]. In the noiseless limit this is expected to happen for $\Omega_M \simeq 2v_0/x_L$, in good agreement with our data for low D_0. Accordingly, by closing its orbit inside a compartment, the swimmer gets trapped there, which explains the sudden drop of η for $\Omega \gtrsim \Omega_M$. The peak in the curves $\bar{v}$ versus ϵ for $\epsilon > 1$ and constant Ω reported in Fig. 3(a) can be interpreted in the same way.

As argued above and shown in Fig. 2, increasing Ω with $\Omega\tau_\theta \gg 1$ and $\Omega < \Omega_M$ helps the self-propulsion velocity align itself parallel to the channel walls ($\bar{v}$ increases), while for $\Omega > \Omega_M$ the JP performs an effective Brownian motion by diffusing away from the walls ($\bar{v}$ decreases). On the other hand, thermal noise disrupts the boundary flows by kicking the particle inside the compartment. It also deform its closed orbits by making them spiral faster and their centers diffuse. As a consequence, on increasing D_0 the Ω peak tends to shift to higher Ω (i.e., smaller R_Ω) and diminish in height, as shown in Fig. 4.

V. RECTIFICATION BY AN EXTERNAL TORQUE

For the sake of a comparison, we now briefly analyze an instance where the torque acting on the microswimmer is externally applied. Let us consider a nonchiral JP of unit charge diffusing in the plane (x,y), subject to a magnetic field B. The Langevin equations (1) can be easily modified to account for the magnetic (Lorentz) force $(B\dot{y}, -B\dot{x})$. The new set of Langevin equations reads

$$\begin{aligned}
\ddot{x} &= -\gamma\dot{x} + B\dot{y} + F_0\cos\theta + \sqrt{\gamma kT}\xi_x(t),\\
\ddot{y} &= -\gamma\dot{y} - B\dot{x} + F_0\sin\theta + \sqrt{\gamma kT}\xi_y(t),\\
\dot{\theta} &= \xi_\theta(t),
\end{aligned} \tag{4}$$

where F_0 denotes the modulus of the effective self-propulsion force and the noises $\xi_x(t)$, $\xi_y(t)$, and $\xi_\theta(t)$ are defined as in Eq. (1). Note that here the self-propulsion speed is $v_0 = F_0/\gamma$, whereas the intrinsic torque was set to zero, $\Omega = 0$. The magnetic force tends to bend the particle trajectory very much like Ω did in the model of Sec. II. In this spirit and following the notation of Ref. [20], we refer to B as an external torque.

The external torque of Eq. (4) has opposite chiral effects than the intrinsic torque of Eq. (1). Indeed, for $B > 0$ ($B < 0$) the magnetic force applies a clockwise (counterclockwise) rotation on the active Brownian trajectories, thus affecting the particle dynamics, especially in the vicinity of the channel walls [19]. This causes a spatial symmetry-breaking mechanism capable of rectifying a confined time-correlated Brownian motion [20]. However, one notes immediately that in the regime of large damping (overdamped limit) effects due to the external torque are strongly suppressed; hence, the need of explicitly incorporating inertia in the particle dynamics of Eq. (4). This is a first important difference with respect to the diffusion properties of chiral JPs investigated sofar.

The numerical results reported in Fig. 5 have been obtained by varying the geometry of the 2D channel of Eq. (2). The outcome of our simulations can be summarized as follows:

(i) Like for chiral JPs, rectification of a magnetic microswimmer also occurs in right-left symmetric channels with broken upside-down symmetry. Moreover, we checked numerically that, as anticipated above, the rectification power drops to zero on increasing either γ [Fig. 5(c)] or D_θ; the decay laws are respectively $1/\gamma^3$ for $\gamma \to \infty$ and τ_θ^2 for $\tau_\theta \to \infty$ (not shown). This is a consequence of the fact that self-diffusion scales like $D_s = \tau_\theta F_0^2/4\gamma^2$; in the limit $\gamma \to \infty$, or $\tau_\theta \to 0$, D_s is suppressed with respect to $D_0 = kT/\gamma$, $D_s/D_0 \propto \tau_\theta/\gamma \ll 1$, so that diffusion is dominated by equilibrium thermal noise, which cannot be rectified.

(ii) Rectification is governed by compartment convexity. In the panels (a) (inset) and (b) of Fig. 5 we report simulation results for a half sinusoidal channel, where the upper wall was taken straight and the lower one sinusoidally corrugated, i.e., $\epsilon = 0$. No matter how large the width, y_L, the net current, $\bar{v}$, is negative. On exchanging $w_+(x)$ with $w_-(x)$, i.e., under $y \to -y$ reflection, the rectification current reverses sign. A qualitative explanation of this behavior is simple. For $B > 0$ the JP behaves like a dextrogyre swimmer; under the action of the external magnetic force, the particle tends to slide to the left against the upper wall and to the right against the lower wall. Our numerical observations support the argument of Sec. III that straight walls have a stronger rectification power than corrugated walls [see Eq. (3)]. The two current reversals shown by the curves $\bar{v}(\epsilon)$ in Fig. 5(a) are thus the result of the competing rectification powers of the upper (to the left, negative) and the lower wall (to the right, positive). For $\epsilon = 1$ the channel compartment is centrosymmetric and, therefore, $\bar{v}$ is identically zero. For $\epsilon < 1$ $w_+(x)$ is less convex than $w_-(x)$, so that $\bar{v} < 0$; for $\epsilon > 1$ the opposite is true and $\bar{v}$ turns positive. However, on further increasing ϵ, the corrugation of $w_+(x)$ grows in amplitude to the point that the diffusing JP gets trapped against the wall; rectification to the right is thus suppressed and $\bar{v}$ reverses sign one last time. This is also why the modulus of $\bar{v}$ in the inset attains a maximum at a certain value of y_L, apparently proportional to Δ. This is another important difference with respect to the intrinsic torque model of Sec. II. In both cases positive torques, $\Omega > 0$ and $B > 0$, yield negative rectification currents, $\bar{v}(\epsilon) < 0$, for $\epsilon < 1$; however, in Fig. 3(a) the JP is levogyre, whereas in Fig. 5(a) it is dextrogyre. Clearly, intrinsic torques and external torques, combined with inertia, produce opposite boundary flows.

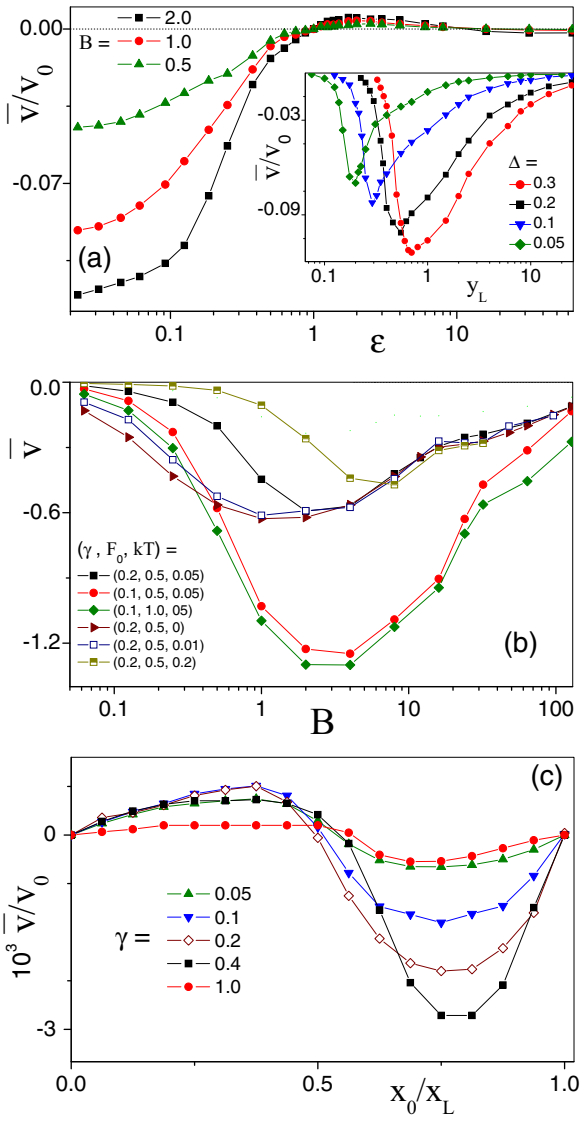

FIG. 5. (Color online) (a) Rectification of a Janus particle in a $x \to -x$ mirror symmetric channel in the presence of torque: $\bar{v}/v_0$ vs ϵ for $D_\theta = 0.3$, $\gamma = 0.2$, $F_0 = 0.5$, $kT = 0.05$, and different values of B. The channel boundaries are described by Eq. (2) with $x_L = y_L = 1$, $\Delta = 0.1$, and $x_0 = 0$. Inset: $\bar{v}/v_0$ vs y_L for $B = 1$, $\epsilon = 0$ (half a sinusoidal channel) and different Δ. The remaining parameters are as in the main panel; (b) $\bar{v}$ vs B for $D_\theta = 0.03$ and different values of γ, F_0, and kT (see legend). Units are as in Eq. (4) and the channel boundaries as in Eq. (2) with $\epsilon = 0$ (half a sinusoidal channel), $x_L = y_L = 1$, and $\Delta = 0.12$; (c) rectification of an inertial Janus particle in an asymmetric channel at zero torque, $B = 0$: $\bar{v}/v_0$ vs x_0 for different γ. $w_\pm(x)$ are given by Eq. (2) for $x_L = y_L = 1$, $\epsilon = 0.25$, and $\Delta = 0.12$; other simulation parameters are $F_0 = 0.5$, $kT = 0.05$, and $D_\theta = 0.3$.

(iii) The dependence on the torque is resonantlike. The curves of $\bar{v}$ versus B displayed in Fig. 5(b) should be compared with the curves of Fig. 4. For $B \to 0$ the instantaneous curvature radius of the stochastic trajectories grows so large in comparison with the compartment size, that its impact on the particle dynamics becomes negligible. Vice versa, for $B \to \infty$ the curvature radius is so much smaller than the pore size, that the diffusive dynamics of the JP is dominated by thermal noise. However, in contrast to Fig. 4, here rectification is the strongest for $\Omega_M \simeq 2\sqrt{kT}/\Delta$. This is consistent with the optimal transport condition that the radius of curvature, $R_\Omega = \sqrt{kT}/\Omega$, associated with the thermal velocity, $v_{\rm th} = \sqrt{kT}$, is of the order of the pore half-width, $\Delta/2$. This condition holds at relatively low damping, as long as $\gamma \ll \Omega_M$ [32].

(iv) Collisions on the upper and lower channel walls are correlated. In the presence of inertia this property holds even for nonchiral Brownian particles [32]. In panel (c) of Fig. 5 we report simulation data for the Brownian dynamics of Eqs. (4) and (2) with $B = 0$ (no torque), $\epsilon = 1/4$ (different wall corrugations amplitudes), and varying x_0 (i.e., shifting the channel walls relative to one another). As discussed in Sec. III, the net current vanishes identically at $x_0^{(n)}/x_L = n/2$, with n integer, where the channel unit cell is centrosymmetric; in the neighborhood of these zeros, $\bar{v}$ is an odd function of x_0. The additional current inversions occurring between two consecutive $x_0^{(n)}$ are not symmetry determined, but rather depend on the dynamical parameters γ and D_θ. Increasing γ shortens both the thermal length, $l_{\rm th} = v_{\rm th}/\gamma$, and the self-propulsion length of the diffusing particle, $l_\theta = \tau_\theta F_0/\gamma$. Note that the ratio $l_{\rm th} = l_\theta$ is independent of γ. As $l_{\rm th}$ grows smaller than the width of the compartment pores, $l_{\rm th} \ll \Delta$, inertia can no longer be invoked to explain rectification; any residual net current must be attributed to the overdamped self-propulsion mechanism introduced in Ref. [23]. Of course this is possible only when l_θ is still comparable with the compartment size, i.e., $l_\theta \gg \Delta \gg l_{\rm th}$. For the simulation parameters of Fig. 5(c), such condition occurs for $2 \lesssim \gamma \lesssim 20$: Nevertheless, no appreciable rectification current was detected for $\gamma > 1$. This is an instance of *accidental* suppression of the rectification mechanism, due to the fact that the channel cross section $\sigma(x) = w_+(x) - w_-(x)$ is sinusoidally modulated and, therefore, itself right-left symmetric [22,24].

VI. CONCLUSIONS AND OUTLOOKS

Diffusion of chiral microswimmers can be rectified even in highly symmetric geometries as an effect of opposite oriented boundary flows. This mechanism can be extended to 3D channels [14]. The "minimum spatial asymmetry" required to generate an autonomous current is that the channel walls have different corrugation.

As a natural extension of our boundary flow approach, we notice that rectification of chiral microswimmers also occurs in different geometries, such as the annulus of radii R_1 and R_2, with $\Delta R = R_1 - R_2 > 0$, illustrated in Fig. 6. A levogyre JP trapped in such a ring tends to drift counterclockwise with angular velocity, $\bar{\omega}_\theta = \langle \dot{\theta} \rangle > 0$. The optimal rectification torque in a thin ring with $\Delta R \ll R_1$ is determined by the condition $R_\Omega = R_1$, i.e., $|\Omega| = \omega_1$ with $\omega_1 = v_0/R_1$. In this limit the particle density across the annulus is uniform, no boundary flows

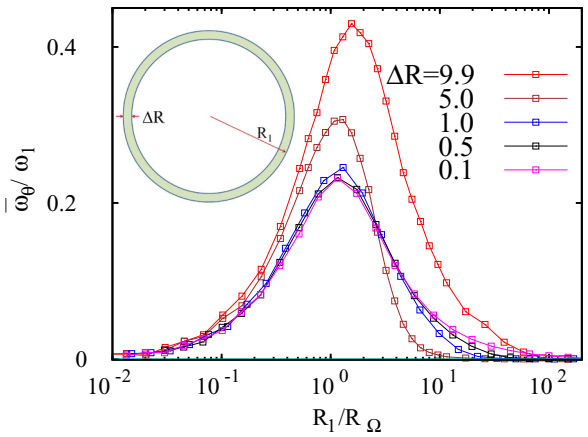

FIG. 6. (Color online) Rectification of a levogyre JP in an annulus of outer radius $R_1 = 10$ and width $\Delta R = R_1 - R_2$ (see sketch) as a function of Ω: net angular velocity, $\bar{\omega}_\theta$ vs R_1/R_Ω, for $\tau_\theta = 20$, $D_0 = 0.01$, $v_0 = 1$, and different ΔR. Here, $R_\Omega = v_0/\Omega$ and $\omega_1 = v_0/R_1 = 0.1$, i.e., $R_1/R_\Omega = \Omega/\omega_1$.

were observed. On the contrary, as the inner radius shrinks so that $\Delta R \to R_1$, the maximum rectification occurs for $R_\Omega \simeq 2\Delta R$. This is the optimal rectification condition illustrated in the central panel of Fig. 2 and discussed in Sec. IV for a directed sinusoidal channel: Opposite boundary flows emerge tangential to the outer (counterclockwise) and inner walls (clockwise), with the former much stronger than the latter. (Notice that in the situation simulated here, the swimmer self-propulsion length l_θ is of the order of R_1.) A simple qualitative argument, introduced in Ref. [33] for the case of charged Brownian particles diffusing in circular confining geometries subjected to a constant magnetic field, also provides an estimate for the upper and lower bounds of the maxima of the curves $\bar{\omega}_\theta/\omega_1$ plotted in Fig. 6, respectively, $1/2$ for $R_2 \to 0$ and $1/4$ for $R_2 \to R_1$, in close agreement with our numerical findings. The reader is referred to that earlier work for more details.

The results discussed in this paper suggest the conceptual design of devices for manipulating chiral JPs. For instance, if a mixture of levogyre (L) and dextrogyre (D) JPs is forced through two openings of appropriate geometry, the annulus investigated in Fig. 6 may be used to separate the two mixture fractions according to their chirality. Moreover, a sieve formed by N cascaded such units, as sketched in Fig. 7, would be selective toward the sign and magnitude of Ω and, more importantly, its efficiency enhanced by increasing N.

This and other applications of chiral rectification surely are within the capabilities of the current technology. Specialized microfluidic circuits can be designed, for instance, to guide chiral microswimmers to a designated target. Taking advantage of the fact that the proposed mechanism is quite sensitive to the degree of chirality of the diffusing particles (engineered or accidental, alike), this effect can be utilized to fabricate monodisperse chiral microswimmers (presently a challenging technological task). By the same token, microswimmers capable of inverting chirality upon binding to a load, can operate as chiral shuttles along a suitably corrugated channel even in the absence of gradients of any kind.

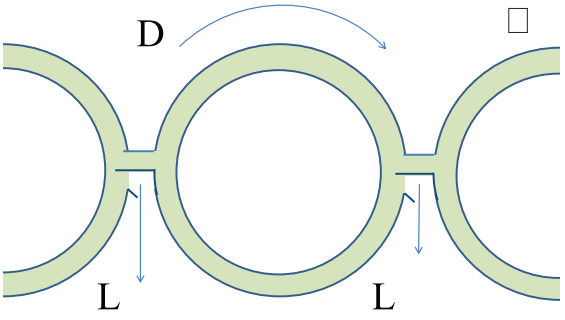

FIG. 7. (Color online) Sketch of a chiral sieve consisting of cascaded rings: As a mixture of levogyre (L) and dextrogyre JPs (D) is pumped from left to right, the levogyre JPs are selectively removed at the links.

The simple model analyzed here was aimed at stressing the role of chirality on active transport in narrow channels. However, to ensure a detailed comparison with the data from ongoing experiments, one should address other important effects: (i) *Hydrodynamic effects*: In this work we ignored the role of the suspension fluid flowing around the moving microswimmer. An accurate account of microfluidic effects is likely to selectively impact the particle boundary flows along a corrugated channel wall as well as the translocation of *finite* size JPs through a narrow pore. (ii) *Wall interactions*: The sliding b.c. implemented in our simulation code are known to reproduce rather closely certain experimental conditions [8], but surely are not granted for all setups under investigation [12,34]. Particle translocation through narrow constrictions may be extremely sensitive to the particle-wall interactions and thus affect active transport in corrugated channels. These issues are the focus of ongoing research.

ACKNOWLEDGMENTS

This work was supported by the NSF China under Grant No. 11334007. Y.L. is also supported by the NSF China under Grants No. 11347216 and No. 11334007, and by Tongji University under Grant No. 2013KJ025.

[1] E. M. Purcell, Am. J. Phys. **45**, 3 (1977).
[2] F. Schweitzer, *Brownian Agents and Active Particles* (Springer, Berlin, 2003); S. Ramaswamy, Annu. Rev. Condens. Matter Phys. **1**, 323 (2010); P. Romanczuk, M. Bär, W. Ebeling, B. Lindner, and L. Schimansky-Geier, Eur. Phys. J. Spec. Top. **202**, 1 (2012); T. Vicsek and A. Zafeiris, Phys. Rep. **517**, 71 (2012).
[3] See, e.g., Y. Hong, D. Velegol, N. Chaturvedi, and A. Sen, Phys. Chem. Chem. Phys. **12**, 1423 (2010).
[4] *Janus Particle Synthesis, Self-Assembly and Applications*, edited by S. Jiang and S. Granick (RSC Publishing, Cambridge, 2012); A. Walther and A. H. E. Müller, Chem. Rev. **113**, 5194 (2013).
[5] W. F. Paxton, S. Sundararajan, T. E. Mallouk, and A. Sen, Angew. Chem., Int. Ed. **45**, 5420 (2006).
[6] J. G. Gibbs and Y.-P. Zhao, Appl. Phys. Lett. **94**, 163104 (2009); J. R. Howse, R. A. L. Jones, A. J. Ryan, T. Gough, R. Vafabakhsh, and R. Golestanian, Phys. Rev. Lett. **99**, 048102 (2007).
[7] H. R. Jiang, N. Yoshinaga, and M. Sano, Phys. Rev. Lett. **105**, 268302 (2010).
[8] G. Volpe, I. Buttinoni, D. Vogt, H.-J. Kümmerer, and C. Bechinger, Soft Matter **7**, 8810 (2011).
[9] L. Baraban, R. Streubel, D. Makarov, L. Han, D. Karnaushenko, O. G. Schmidt, and G. Cuniberti, ACS Nano **7**, 13602013.
[10] B. M. Friedrich and F. Jülicher, Phys. Rev. Lett. **103**, 068102 (2009).
[11] A. Búzás, L. Kelemen, A. Mathesz, L. Oroszi, G. Vizsnyiczai, T. Vicsek, and P. Ormos, Appl. Phys. Lett. **101**, 041111 (2012).
[12] S. van Teeffelen and H. Löwen, Phys. Rev. E **78**, 020101 (2008).
[13] C. J. Brokaw, J. Exptl. Biol. **35**, 197 (1959); J. Cell. Comp. Physiol. **54**, 95 (1959).
[14] M. Mijalkov and G. Volpe, Soft Matter **9**, 6376 (2013).
[15] F. Kümmel, B. ten Hagen, R. Wittkowski, I. Buttinoni, R. Eichhorn, G. Volpe, H. Löwen, and C. Bechinger, Phys. Rev. Lett. **110**, 198302 (2013).
[16] A. Boymelgreen, G. Yossifon, S. Park, and T. Miloh, Phys. Rev. E **89**, 011003(R) (2014).
[17] A. Sen, M. Ibele, Y. Hong, and D. Velegol, Faraday Discuss. **143**, 15 (2009).
[18] A. Zöttl and H. Stark, Phys. Rev. Lett. **108**, 218104 (2012).
[19] T. R. Kline, W. F. Paxton, T. E. Mallouk, and A. Sen, Angew. Chem., Int. Ed. **44**, 744 (2005).
[20] P. K. Radtke and L. Schimansky-Geier, Phys. Rev. E **85**, 051110(R) (2012).
[21] S. Sengupta, M. E. Ibele, and A. Sen, Angew. Chem., Int. Ed. **51**, 8434 (2012).
[22] P. Hänggi and F. Marchesoni, Rev. Mod. Phys. **81**, 387 (2009).
[23] P. K. Ghosh, V. R. Misko, F. Marchesoni, and F. Nori, Phys. Rev. Lett. **110**, 268301 (2013).
[24] For a review, see P. S. Burada, P. Hänggi, F. Marchesoni, G. Schmid, and P. Talkner, ChemPhysChem **10**, 45 (2009).
[25] M. Ripoll, P. Holmqvist, R. G. Winkler, G. Gompper, J. K. G. Dhont, and M. P. Lettinga, Phys. Rev. Lett. **101**, 168302 (2008).
[26] D. Takagi, J. Palacci, A. B. Braunschweig, M. J. Shelley, and J. Zhang, Soft. Matter **10**, 1784 (2014).
[27] I. Buttinoni, J. Bialkè, F. Kümmel, H. Löwen, C. Bechinger, and T. Speck, Phys. Rev. Lett. **110**, 238301 (2013).
[28] Y. Fily and M. C. Marchetti, Phys. Rev. Lett. **108**, 235702 (2012).
[29] Y. Fily, A. Baskaran, and M. F. Hagan, Soft Matter **10**, 5609 (2014).
[30] For a minireview, see X. Ao, P. K. Ghosh, Y. Li, G. Schmid, P. Hänggi, and F. Marchesoni, arXiv:1409.5061 [Eur. Phys. J. Spec. Top. (to be published)].
[31] P. K. Ghosh, P. Hänggi, F. Marchesoni, S. Martens, F. Nori, L. Schimansky-Geier, and G. Schmid, Phys. Rev. E **85**, 011101 (2012).
[32] P. K. Ghosh, P. Hänggi, F. Marchesoni, F. Nori, and G. Schmid, Europhys. Lett. **98**, 50002 (2012); Phys. Rev. E **86**, 021112 (2012).
[33] A. Pototsky, P. Hänggi, F. Marchesoni, and S. Savel'ev, Phys. Rev. E **84**, 011107 (2011).
[34] W. E. Uspal, M. N. Popescu, S. Dietrich, and M. Tasinkevych, arXiv:1407.3216.